The impact of vent geometry on the growth of lava domes

Catherine Mériaux, Dave May, Claude Jaupart

Geophysical Journal International

Geophys. J. Int. (2022) **229,** 1680–1694
Advance Access publication 2022 January 07
GJI Heat Flow and Volcanology

https://doi.org/10.1093/gji/ggac005

The impact of vent geometry on the growth of lava domes

Catherine.A. Mériaux [1,2,3] Dave A. May[4] and Claude Jaupart[5]

[1] *School of Earth, Atmosphere and Environment, Monash University, 9 Rainforest Walk Clayton, Victoria 3800, Australia. E-mail: cmeriaux@eaifr.org*
[2] *The Abdus Salam International Centre for Theoretical Physics (ICTP) Strada Costiera, 11 - I-34151 Trieste, Italy*
[3] *ICTP-East African Institute for Fundamental Research, KIST2 Building CST, Nyarugenge Campus, University of Rwanda, KN 7 Avenue, Kigali, Rwanda*
[4] *Institute of Geophysics and Planetary Physics, Scripps Institution of Oceanography, University of California San Diego, La Jolla, CA 92037, USA*
[5] *Institut de Physique du Globe de Paris, 1, rue Jussieu - 75238 Paris cedex 05, France*

Accepted 2022 0. Received 2021 December 4; in original form 2021 July 21

SUMMARY

Thick lava flows that are a feature of many volcanic fields on the Earth and Venus vary from sheet-like to nearly perfect axisymmetric domes. Here, we investigate how these geometrical characteristics depend on the shape of the feeder vent. We study the gravitational spreading of viscous lava erupting from elliptical vents onto a flat surface using 3-D numerical models. The aspect ratio of the vent, defined to be the major to minor axes ratio, varies between 1 and 25. In the limit of an aspect ratio of one, the vent is circular and spreading is axisymmetric. In the limit where the ratio is large, the vent behaves as a fissure. The numerical models rely on an isoviscous lava rheology and a constant volumetric eruption rate. In all cases, the initial phase of the dome's evolution is in a lava-discharge dominated regime such that spreading is insignificant and the height of the dome increases at a constant rate over the vent area. For vent aspect ratios greater than five, three successive regimes of spreading are identified: 2-D spreading in the direction perpendicular to the major axis of the vent, a transient phase such that the dome shape evolves towards that of a circular dome and a late axisymmetric spreading phase that does not depend on the vent shape. These regimes are delimited by the times required for the flow thickness above the vent to reach a given height and for the flow to spread axisymmetrically up to a length equal to the semi-major axis of the vent. Numerical results for the flow height and runout length tend towards the similarity solutions in the 2-D and axisymmetric regimes. Two main implications for highly viscous (rhyolitic) fissure eruptions can be drawn. First, the fissure length determines the flow regimes. The longer the vent fissure length, the longer the early lava discharge regime and 2-D spreading perpendicular to the length of the fissure. Second, the aspect ratio of fissure-fed lava flows can be used as an indicator of the fissure length and the duration of lava discharge. The ellipticity of some terrestrial fissure-fed flows provides evidence for viscous gravity-driven spreading terminated before the onset of the axisymmetric regime. On the other hand, the circular domes on Venus appear to be the result of fissure-fed eruptions sustained enough for the spreading to reach the axisymmetric regime. We propose relationships providing estimates of the fissure length and the duration of lava discharge based on fossil dome dimensions.

Key words: Numerical modelling; Planetary volcanism; Eruption mechanisms and flow emplacement.

1 INTRODUCTION

On the Earth, chains of volcanoes established above subducting plates also known as volcanic arc are prone to generate lava domes. The latter typically form during the eruption of highly viscous lavas from a volcanic vent onto flat surfaces. Due to the high viscosity, they spread slowly over a limited spatial area compared to low-viscosity lava flows. Yet, lava domes are potentially deadly because when they collapse, they generate pyroclastic flows. They are thus considered to be precursors of potential large explosive eruptions (e.g. Mount Pelée, Martinique, 1902). The dynamics of lava domes has thus received a lot of attention.

Although lava domes are often represented as circular mounds, field studies have shown that they exhibit a variety of shapes and sizes that include platy, blocky and lobate domes and spines (Fink & Anderson 2000). Types of lava dome morphology have been distinguished depending, among others, on the lava flow effusion rate at the vent and the viscosity of lava and its temperature dependence

(e.g. Rhodes *et al.* 2018). Two types of growth have also been described: endogenous growth caused by intrusion of new magma and exogenous growth due to magma forcing its way through a brittle cooled lava carapace at the surface forming discrete lobes (e.g. Kaneko *et al.* 2002).

Besides, many lava domes grow in a preferred direction (e.g. Pallister *et al.* 2013). Such a deviation from the axisymmetric geometry has been attributed to the topographic context where the dome is emplaced, such as on a slope (Diefenbach *et al.* 2013), or changes in the local stress fields (Zorn *et al.* 2019). A number of studies have also documented the existence of elongated and circular lava domes or coulee that were linked or connected to a fissure vent or a tabular conduit (e.g. Fink & Pollard 1983; Sieh & Bursik 1986; Aguirre-Díaz & Labarthe-Hernández 2003; Waite *et al.* 2008; Kósik *et al.* 2019; Leggett *et al.* 2020). The presence of fissure vents is mostly inferred from the shape of the dome and surrounding observations as direct observations are prevented by the lava covering the vent. Drilling has been carried out as in the Obsidian Dome (Eichelberger *et al.* 1984), but the information remained localized in space and insufficient to characterize the vent. Lava domes or coulees considered issued from fissure vents can be isolated such as the Douglas Knob (Christiansen *et al.* 2007; Befus *et al.* 2014), but more often, they are aligned in clusters along tectonic or volcano-tectonic lineaments parallel to the nearby faults. In these environments, grabens result from dyke intrusions and normal faulting indicating a regional extensional stress field. Tensile cracks can also be observed around the domes. Examples of such clusters include the Taylor Creek Rhyolite Domes, the Mono-Inyo Crater or the Puketerata Volcanic Domes (see for instance Loney 1968; Brooker *et al.* 1993; Duffield *et al.* 1995). However, the rationale behind lava dome asymmetry and the dynamics of rhyolitic (highly viscous) fissure eruptions is still poorly understood.

Laboratory and numerical modelling of lava domes have largely supported field observations highlighting the importance of the cooling mechanisms of the dome top surface, the effusive flow rate and the lava rheological model for lava (e.g. Fink & Griffiths 1998; Blake & Bruno 2000; Lyman *et al.* 2004; Hale *et al.* 2007; Tsepelev *et al.* 2020). The effects of changes in vent geometry on the dynamics of spreading and its influence on lava flows, including lava domes, were studied by Fink & Griffiths (1992) and Griffiths & Fink (1993). The latters however compared only two limits: a circular vent and a narrow slit, that is an infinitely long fissure, without elaborating on the difference between the two types of vent and on the implications that vents of intermediate geometry would have. Costa *et al.* (2007) studied lava extrusions from a fissure of finite dimensions but at depth, the latter being connected to a cylindrical conduit terminated by a circular vent at shallower depths and at the surface. In the case of fissure eruptions, Jones & Llewellin (2021) recently showed the likelihood of a localization of the fissure at the eruptive vent without going into details on the geometry of the vent. To our knowledge, no systematic study has focused on the role of vent geometry on the growth of lava domes in cases other than a circular vent or a narrow slit. Filling this gap has been the motivation of this study. For that purpose, we employed 3-D numerical simulations as the method of choice. In practice, we considered the endogenous growth mode and explored the impact of a finite non-circular geometry of the vent on the spreading of isoviscous lava domes adopting an elliptical vent, the aspect ratio of which we varied up to a factor 25. We used a feeding condition where the volume flux (also referred to as the lava discharge rate or the effusive flow rate) at the vent is fixed. As lava domes spread due to gravity while being retarded by internal viscous forces, they involve the propagation of viscous gravity-driven currents. Therefore, we also used as a reference the theoretical framework of similarity solutions for the propagation of such currents (Huppert 1982; Lister & Kerr 1989). We will show that our approach has also the advantage of characterizing the initial phase of eruption involving insignificant spreading, a phase which has been poorly described until now.

2 METHODS

2.1 Model setup

The model is composed of a horizontal 'air' layer of length, height and width in the respective directions x, y and z, L_x, L_y and L_z and an elliptical vent that is located at the base of the air layer and from which lava originates and spreads like a viscous gravity current over a rigid surface. The lava density ρ_l is much greater than that of the air, ρ_a, which is considered to be null. Both fluids have a Newtonian viscosity but the viscosity of lava μ_l is much greater than that of the air, μ_a.

The lava discharge is characterized by a vertical velocity profile of Poiseuille flow $v_y(x, 0, z)$ originating from the elliptical vent. The vent position is located at the base of the domain ($y = 0$) at the position $(x_v, 0, z_v)$ and its area is $\pi r_x^0 r_z^0$, where r_x^0 is the semi-major axis along the x-axis and r_z^0 is the semi-minor axis of the elliptical vent along the z-axis. At the vent, the velocity $v_y(x, 0, z)$ is thus given by

$$v_y(x,0,z) = \frac{2Q}{\pi r_x^0 r_z^0}\left[1 - \frac{(x-x_v)^2}{(r_x^0)^2} - \frac{(z-z_v)^2}{(r_z^0)^2}\right] \quad \text{when } \frac{(x-x_v)^2}{(r_x^0)^2} + \frac{(z-z_v)^2}{(r_z^0)^2} \le 1, \tag{1}$$

$$v_y(x,0,z) = 0 \text{ when } \frac{(x-x_v)^2}{(r_x^0)^2} + \frac{(z-z_v)^2}{(r_z^0)^2} > 1, \tag{2}$$

where Q is the volume flux feeding the dome. In the limit $r_x^0 = r_z^0$, the vent is circular. In the limit $r_x^0 \gg r_z^0$, the vent is a fissure. The volume flux Q is fixed over the entire evolution of the dome. At any time $t \ge 0$, the volume of the dome V is therefore given by $V = Qt$.

The system is characterized by a very small Reynolds number $Re = \rho_l U L/\mu_l$, where L and U are respectively the characteristic length and velocity scales. If we assume $L = r_x^0 = 50$ m, $Q = 10$ m^3 s^{-1}, $U = Q/\pi(r_x^0)^2 = 10/(\pi\ 50^2)$ m s^{-1}, $\rho_l = 2400$ kg m^{-3} and $\mu_l = 10^{11}$ Pa s, $Re = 1.5 \times 10^{-9}$. The lava flow therefore occurs in a laminar regime and inertia can be neglected.

The model is a simplification of volcanic systems. In particular, it is isothermal and isoviscous, which means that the assumed rheological behaviour for the lava and air will be independent of both temperature and stress. The lava viscosity μ_l thus represents an effective viscosity, which takes into account the high-viscosity layer which forms from the surface of the dome due to cooling as it flows. Such effective viscosity is therefore substantially larger than the viscosity estimate based on the lava temperature and composition (Huppert *et al.* 1982; Stasiuk *et al.* 1993). Huppert *et al.* (1982) for example indicated a ratio of 9523 between the two viscosities for the lava of the Soufrière of St Vincent. Lavas dome may contain volatiles but the effects of gas bubbles and compressibility, including crystallization induced by degassing, is typically limited and can be accommodated by an increase in the effective viscosity (Jaupart 1991). This simplified design aims to better isolate the influence of the geometry of the vent on the dynamics of spreading while allowing benchmarking with analytic solutions that will be presented in Section 2.3.

2.2 Numerical method and workflow

The lava dome growth initiates a creeping flow ($Re \ll 1$) subject to incompressibility that was described by the Stokes equations given by

$$\nabla \cdot \left[\mu \left(\boldsymbol{v}^T + \boldsymbol{v}\right)\right] - \nabla p = \rho \boldsymbol{g}, \tag{3}$$

$$\nabla \cdot \boldsymbol{v} = 0, \tag{4}$$

where $\boldsymbol{v}$ and p are the fluid velocity and pressure; μ and ρ are the fluid viscosity and density; and $\boldsymbol{g}$ is the gravitational acceleration vector. While eqs (3) and (4) are known to describe a steady-state flow, we introduced time dependence in the flow field through the evolution of the density and viscosity, namely $\rho(\boldsymbol{x}, t)$ and $\mu(\boldsymbol{x}, t)$, respectively. We thus solved the additional evolution equations following a fluid parcel

$$\frac{\mathrm{D}\mu}{\mathrm{D}t} = 0, \tag{5}$$

$$\frac{\mathrm{D}\rho}{\mathrm{D}t} = 0, \tag{6}$$

where D/Dt is the material derivative. In practice, eqs (5) and (6) are solved using the method of characteristics ($d\mu/dt = 0; \mathrm{d}\boldsymbol{x}/\mathrm{d}t = \boldsymbol{v}$).

At the boundaries of the computational domain, eqs (3) and (4) were closed by Dirichlet and Neumann conditions, while eqs (5) and (6) were subject to properties' conditions. In practice, along the base of the domain, we imposed that the velocity satisfies

$$\boldsymbol{v}(\boldsymbol{x}) \cdot \boldsymbol{n} = v_y(x, 0, z), \text{ when } \boldsymbol{x} \in \Gamma_v \tag{7}$$

$$\boldsymbol{v}(\boldsymbol{x}) \cdot \boldsymbol{n} = 0, \text{ when } \boldsymbol{x} \notin \Gamma_v, \tag{8}$$

where Γ_v is the vent domain and $\boldsymbol{n}$ is the outward pointing normal to the bottom surface. We also required that

$$\mu(\boldsymbol{x}, t) = \mu_l \text{ for all } \boldsymbol{x} \text{ where } \boldsymbol{v}(\boldsymbol{x}) \cdot \boldsymbol{n} < 0, \tag{9}$$

$$\rho(\boldsymbol{x}, t) = \rho_l \text{ for all } \boldsymbol{x} \text{ where } \boldsymbol{v}(\boldsymbol{x}) \cdot \boldsymbol{n} < 0. \tag{10}$$

On the left and back boundaries, we imposed symmetry by applying

$$\boldsymbol{v} \cdot \boldsymbol{n} = 0, \tag{11}$$

$$\boldsymbol{t} \cdot \left[\mu \left(\boldsymbol{v}^T + \boldsymbol{v}\right) - p\boldsymbol{I}\right] \cdot \boldsymbol{n} = 0, \tag{12}$$

with no condition on the properties. Along the top, right and front boundaries of the domain, we imposed

$$\boldsymbol{n} \cdot \left[\mu \left(\boldsymbol{v}^T + \boldsymbol{v}\right) - p\boldsymbol{I}\right] \cdot \boldsymbol{n} = 0, \tag{13}$$

$$\boldsymbol{t} \cdot \left[\mu \left(\boldsymbol{v}^T + \boldsymbol{v}\right) - p\boldsymbol{I}\right] \cdot \boldsymbol{n} = 0, \tag{14}$$

which accommodated the volume change due to the lava influx, and

$$\mu(\boldsymbol{x}, t) = \mu_a \text{ for all } \boldsymbol{x} \text{ where } \boldsymbol{v}(\boldsymbol{x}) \cdot \boldsymbol{n} < 0, \tag{15}$$

$$\rho(\boldsymbol{x}, t) = \rho_a \text{ for all } \boldsymbol{x} \text{ where } \boldsymbol{v}(\boldsymbol{x}) \cdot \boldsymbol{n} < 0. \tag{16}$$

In this problem, the flow is allowed to develop over large times and eventually follows asymptotic similarity solutions with dimensions that depend on time. In this case, the relevant scales for time and length are best derived from critical stages in the flow evolution rather than from the initial conditions. This is explained in greater length in Section 2.3 below.

The numerical solution of the time dependent linear Stokes flow problem was obtained using the parallel particle-in-cell finite element code *ptatin3d* (May *et al.* 2014, 2015). The discretized equations were solved using a structured mesh of hexahedral elements employing bi-quadratic and linear-shape (called Q2-P1) elements basis functions for velocity and pressure, respectively. To support efficient computations on parallel computational infrastructure, we employ linear solvers and preconditions for the discrete system of equations using PETSc (Balay *et al.* 1997, 2017, 2022). The solver relied on a Krylov method with an upper block triangular preconditioner. In all simulations, the vent source/centre was located at the origin of the domain, that is $(x_v, y_v, z_v) = (0, 0, 0)$. Consequently, we took advantage of the system symmetry about the x and z axis and halved the computational domain in both directions. As a result, we model a quarter of the dome only.

The numerical grid was uniform in all directions with variable resolutions $\Delta x = L_x/N_x$, $\Delta y = L_y/N_y$, and $\Delta z = L_z/N_z$, where $N_{i=x,y,z}$ is the number of elements in the i direction. Various mesh resolutions were adjusted upon the requirement that the lava volume flux Q_{num} that was numerically calculated and the prescribed volume flux did not differ by more than 3 per cent. Typically, the vent semi-minor and semi-major axes were resolved by a minimum of ∼4 elements in the x and z directions. The Lagrangian swarm was analysed in the simulation time-stepping and post-processing workflow to extract the maximum height of dome $h(t)$, the lava maximum positions of the lava, $r_x(t)$ and $r_z(t)$, in the x and z directions. The three markers $h(t)$, $r_x(t)$ and $r_z(t)$ were used to track the dome evolution. Simulation parameters are detailed in Table 1. The lava/air viscosity contrast was kept constant and equal to 10^3. Such a contrast had been shown to be sufficiently large to minimize the normal and tangential shear stress exerted by the air layer on the dome (Crameri *et al.* 2012).

2.3 Theoretical background and scaling

The propagation of viscous gravity currents from a point or a line source is well described by similarity solutions derived from the Stokes equations and the global continuity equation within the framework of the approximation of the lubrication theory. The approximation requires that the horizontal extent of currents is much larger than their vertical extent so that the vertical velocity component is much smaller than the horizontal velocity components by a factor given by the ratio of the height to the length of the current.

In the limit of a circular feeding vent, the growth of a dome is analogue to that of an axisymmetric viscous gravity-driven current propagating over a rigid surface when $h \ll r_x$ or $h \ll r_z$. At long times, the vent can be considered as a point source, and in the case where it releases a constant volume flux Q, the current evolves as

$$\mathcal{R}_n(t) = 0.715 \left(\frac{\rho_l g Q^3}{3\mu_l}\right)^{1/8} t^{1/2}, \tag{17}$$

$$\mathcal{H}(0) = k_1 \times (0.715)^{2/3} \left(\frac{3Q\mu_l}{\rho_l g}\right)^{1/4}, \tag{18}$$

where $\mathcal{R}_n(t)$ and $\mathcal{H}(0)$ are the radial front and maximum height of the current, respectively (Huppert 1982). Note that $\mathcal{H}(0)$ is independent of time. A multiplicative constant k_1 was added to eq. (18) following calibration with the simulations giving $k_1 = 1.60$. This calibration results from the singularity of the exact solutions at the origin when the volume flux is constant (see Huppert 1982).

The similarity solution given by eqs (17) and (18) is based on the assumption that the flow is controlled by gravity whereas the influence of the pressure gradient ($\propto \mu_l Q/h^3 r$) due to the lava

Table 1. Dimensional parameters of simulations performed at constant volume flux Q. The gravitational acceleration is $g = 9.81$ ms^{-2}.

Simulation Id.	$L_x \times L_y \times L_z$ (m × m × m)	r_x^0 (m)	r_z^0 (m)	Q (m^3 s^{-1})	ρ_l (kg m^{-3})	μ_l (Pa s)	μ_a (Pa s)	t_B/t_Q	T_s (day)	H_s (m)	$N_x \times N_y \times N_z$
VCH	256 × 128 × 256	15	15	17.5	2400	2×10^9	2×10^6	0.61	0.0134	58.8070	64 × 64 × 64
V2Q1R1	256 × 128 × 256	36	18	1.0	2600	2×10^9	2×10^6	0.13	0.6594	28.1824	64 × 64 × 64
V2Q1R0	256 × 128 × 256	32	16	1.0	2400	2×10^9	2×10^6	0.16	0.5210	28.7521	64 × 64 × 64
V5Q1R00	384 × 128 × 384	40	8	1.0	2400	2×10^9	2×10^6	0.29	0.8141	28.7521	128 × 64 × 192
V10Q1R00	384 × 128 × 384	80	8	1.0	2400	2×10^9	2×10^6	0.23	3.2564	28.7521	128 × 64 × 192
V10Q1R0	768 × 128 × 768	160	16	1.0	2400	2×10^9	2×10^6	0.09	13.025	28.7521	128 × 64 × 192
V10Q10R0	768 × 128 × 768	160	16	10.0	2400	2×10^9	2×10^6	0.19	2.3163	51.1292	128 × 64 × 192
V25Q1R0	768 × 128 × 768	400	16	1.0	2400	2×10^9	2×10^6	0.07	81.0490	28.7521	128 × 64 × 192

discharge is small. This condition is satisfied as long as the time t_B it takes to propagate a distance $\mathcal{H}(0)$ is shorter than the time t_Q it takes for the lava discharge to inject the volume $\pi\mathcal{H}(0)(r_x^0)^2$ over the vent, that is $t_B \ll t_Q$, or more explicitly $\mu_l/(\rho_l g\mathcal{H}(0)) \ll \pi\mathcal{H}(0)(r_x^0)^2/Q$.

In the very early times, however the flow is expected to be dominated by the lava discharge with a negligible role of gravity because the horizontal pressure gradient ($\propto \rho_l g \partial h/\partial r$) is not sufficiently large. The discharge then causes the height of the dome to build almost linearly over the finite dimensions of the source while no spreading occurs. This very early-time regime takes place as $t \lessapprox t_Q$ and is characterized by a height evolution that follows $\mathcal{H}(0,t) \approx 2Qt/[\pi(r_x^0)^2]$, assuming that the dome volume is an approximation of the volume of the segment of a sphere defined by $V = \pi h[3(r_x^0)^2 + h^2]/6$.

In the limit of a fissure vent along the x axis, the growth may occur as if it was fed by a line source coinciding with the x axis. The propagation is then assumed as being identical in all the (y, z) planes and therefore 2-D. The similarity solution for a 2-D viscous gravity-driven current propagating over a rigid surface at a constant volume flux per unit of fissure length q is given by

$$\mathcal{Z}_n(t) = \left(\frac{\rho_l g q^3}{3\mu_l}\right)^{1/5} t^{4/5}, \tag{19}$$

$$\mathcal{H}_{2d}(0,t) = 1.325\left(\frac{3q^2\mu_l}{\rho_l g}\right)^{1/5} t^{1/5}, \tag{20}$$

where $\mathcal{Z}_n(t)$ and $\mathcal{H}_{2d}(0,t)$ are the front and maximum height of the current, respectively (Huppert 1982). This solution is valid when $h \ll r_x$ and $h \ll r_z$.

Similar to the axisymmetric case, the solution assumes that the influence of the pressure gradient due to the lava discharge is negligible compared to that of gravity, that is $t_B \ll t_Q$ or $\mu_l/(\rho_l g H_{2d}) \ll H_{2d} r_z^0/q$, where $H_{2d} = 1.325^{4/3}(3q\mu_l/(\rho_l g))^{1/3}$. In the very early times, the reverse is however expected, causing the height of the dome to increase almost linearly with time along the length of the fissure without spreading. The height evolution can then be approximated by $\mathcal{H}(0,t) \approx 2Qt/(\pi r_x^0 r_z^0)$.

In this study, all simulations are characterized by an initial ratio $t_B/t_Q < 1$ (see Table 1). So, except in the very early times, the dynamics is expected to be dominated by gravity. We will show that the solutions (eqs 17 and 18 & 19 and 20) can apply at long and short times, respectively, to the growth of lava domes issued from a fissure-like vent when the volume flux Q is kept constant. We consequently chose to show the results using the characteristics lateral length, height and timescales, L_s, H_s and T_s, to respectively be the semi-major axis of the vent r_x^0, the height $\mathcal{H}(0)$ and the time it would take an axisymmetric dome to propagate up to a radius of length r_x^0, which is given by

$$T_s = \left(\frac{r_x^0}{0.715}\right)^2 \left(\frac{\rho_l g Q^3}{3\mu_l}\right)^{-1/4}. \tag{21}$$

In doing so, we will show departures from the asymptotic similarity solutions to the governing eqs (3) and (4) as a function of the geometry of the vent.

3 RESULTS

3.1 Benchmark of the simulations

Before considering elliptical vents, we performed simulation (VCH) with a circular vent (i.e. $r_x^0 = r_z^0$) for a benchmark against run 1 by Hale *et al.* (2007) and the associated similarity solution $[\mathcal{H}(0), \mathcal{R}_n(t)]$ by Huppert (1982). Fig. 1 shows the evolution of the height and radius of the dome in the three approaches. The evolution of the height does not differ between the two simulations. Both reach a plateau at a dimensionless value $h/H_s = h/\mathcal{H}(0) \sim 1$ as shown in Figs 1(a) and (b). The evolution of the radius measured along both the x and z axis (r_x and r_z) is also similar between the two numerical simulations until a dimensionless time of 35. Beyond this time, from which h/r_x or $h/r_z < 0.67$ (see Fig. 1f), simulation VCH follows the similarity solution by Huppert (1982), whereas run 1 by Hale *et al.* (2007) misses the trend (see Fig. 1c). The very early regime during which the dome height increases almost without radial spreading is well identified by the lava discharge time t_Q (see Figs 1b–d and f).

3.2 Dome evolution

Fig. 2 shows the evolution of the dome at constant volume flux for the slightly fissure-like vent (r_x^0/r_z^0=2; simulation V2Q1R0). The shape of the dome evolves from an elliptical to a circular mound. Its evolution can be summed up in two phases successively characterized by vertical growth with an insignificant horizontal spreading (Figs 2a and b) followed by a horizontal spreading with swelling of the dome from a maximum height which evolves almost no longer from $t = 2T_s$ (Figs 2c–f).

Fig. 3 shows the evolution of the dome at constant volume flux for the most fissure-like vent (r_x^0/r_z^0=25; simulation V25Q1R0). The shape of the dome evolves from a very narrow steep ridge ($t < t_Q$) to a circular mound. Its evolution can be summed up in three main phases successively characterized by vertical growth with insignificant horizontal spreading (Fig. 3a), vertical growth associated with spreading perpendicular to the semi-major axis of the vent (Figs 3b and c) and horizontal spreading with inflation of the dome but constant maximum height (Figs 3d–f).

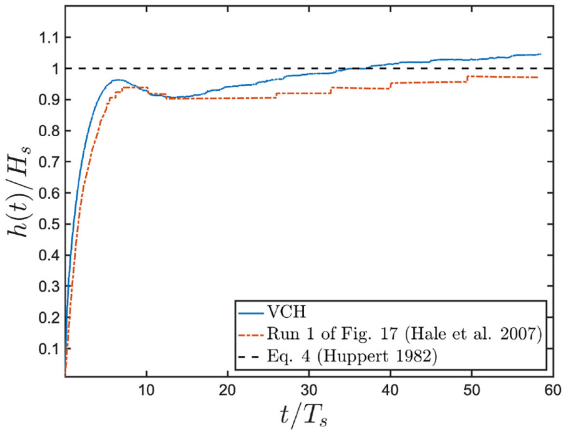

(a) Dimensionless height (linear scale)

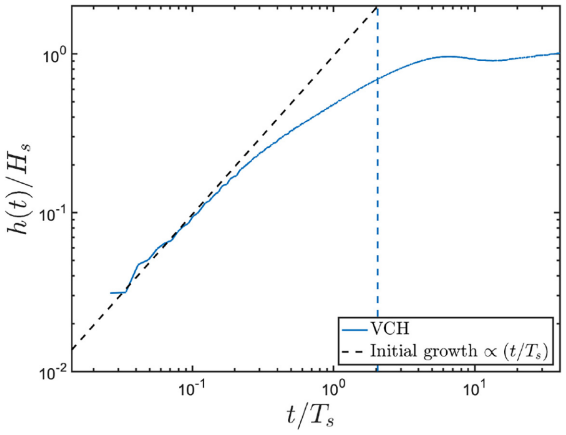

(b) Dimensionless height (log scale)

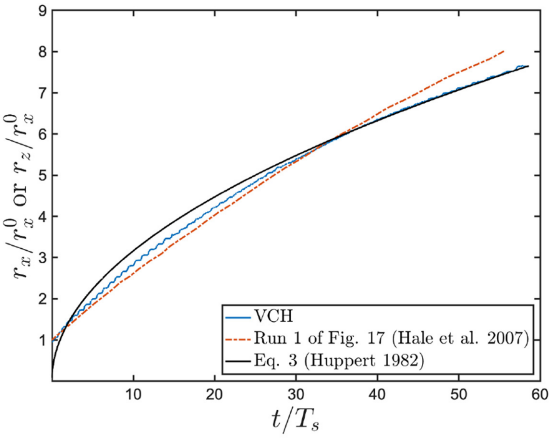

(c) Dimensionless dome length (linear scale)

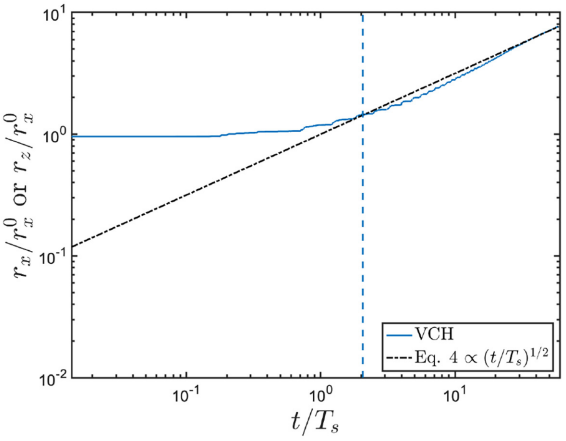

(d) Dimensionless dome length (log scale)

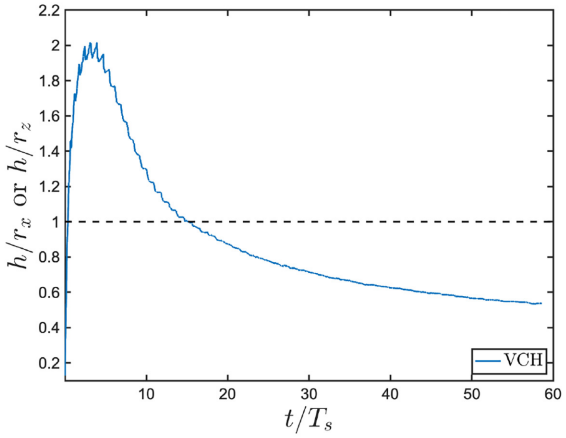

(e) Transverse aspect ratio (linear scale)

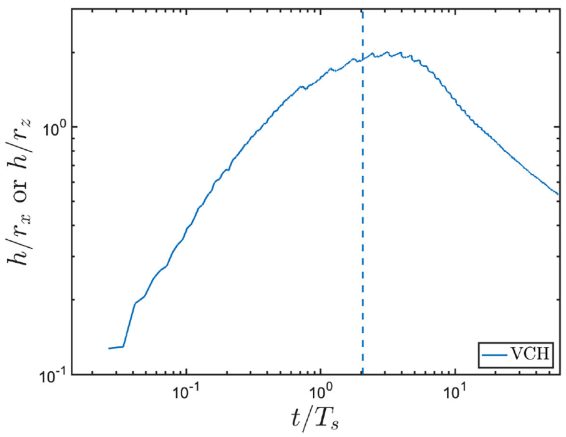

(f) Transverse aspect ratio (log scale)

Figure 1. Benchmark of simulation VCH against run 1 of fig. 17 by Hale *et al.* (2007) and similarity solution by Huppert (1982; eqs 17 and 18). The vertical blue dashed line on the three right-hand panels indicates the lava discharge time $t = t_Q$ defined in Section 2.3. The dashed black line in (b) corresponds to the $h(t)/H_s = 2QT_s/[\pi(r_x^0)^2](t/T_s)$. (For interpretation of the colours in this figure legend, the reader is referred to the web version of this paper.)

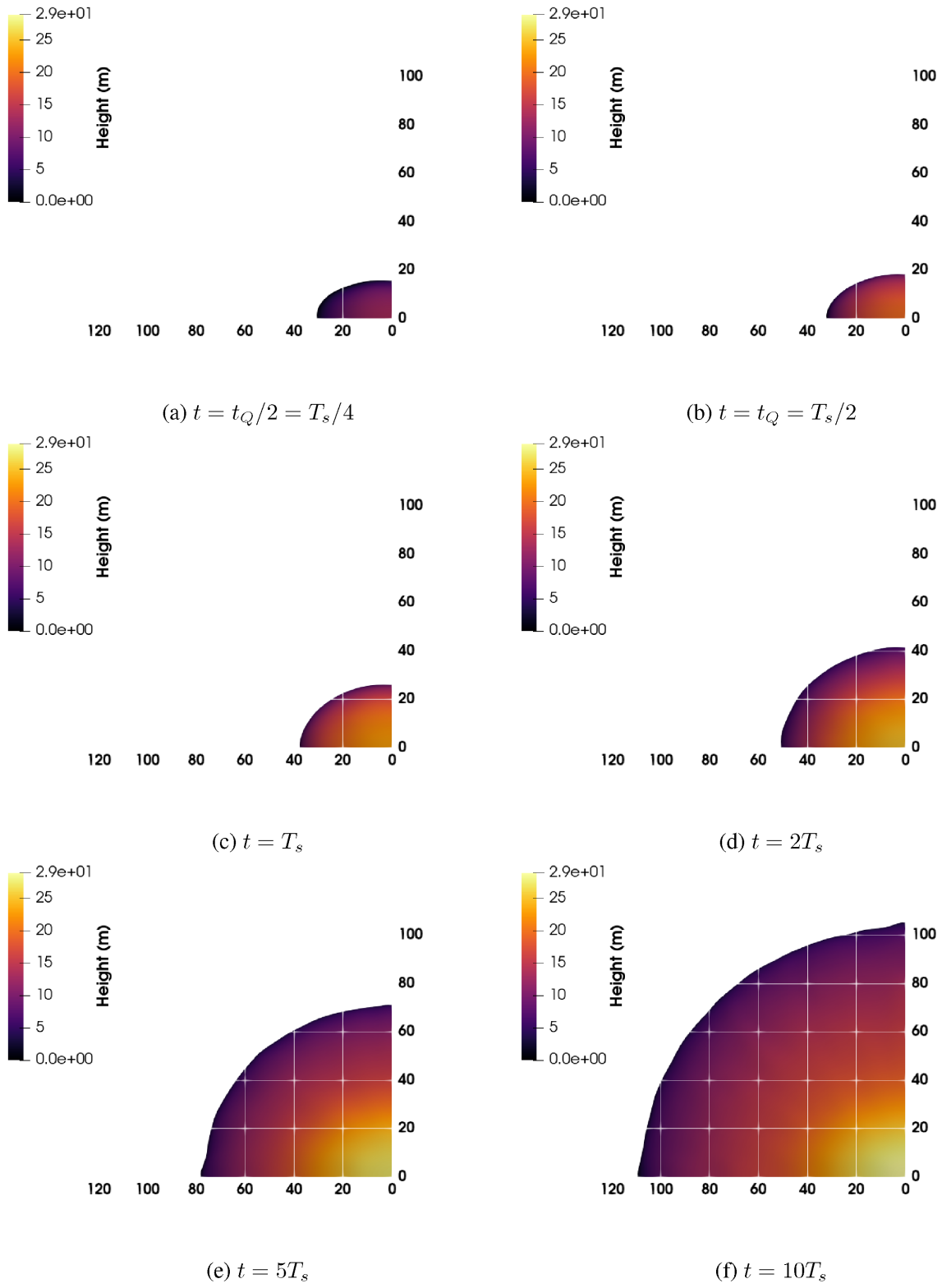

(a) $t = t_Q/2 = T_s/4$

(b) $t = t_Q = T_s/2$

(c) $t = T_s$

(d) $t = 2T_s$

(e) $t = 5T_s$

(f) $t = 10T_s$

Figure 2. Plan view of the evolution of the dome in simulation V2Q1R0. The vent dimensions $r_x^0 \times r_z^0$ were 32 m × 16 m. We recall that only a quarter of the dome has been simulated based on the symmetry. The view direction is perpendicular to the height y and the colours map the height of the dome (in metre). The horizontal and vertical ticks refer to distances in metre. (For interpretation of the references to colour in this figure legend, the reader is referred to the web version of this paper.)

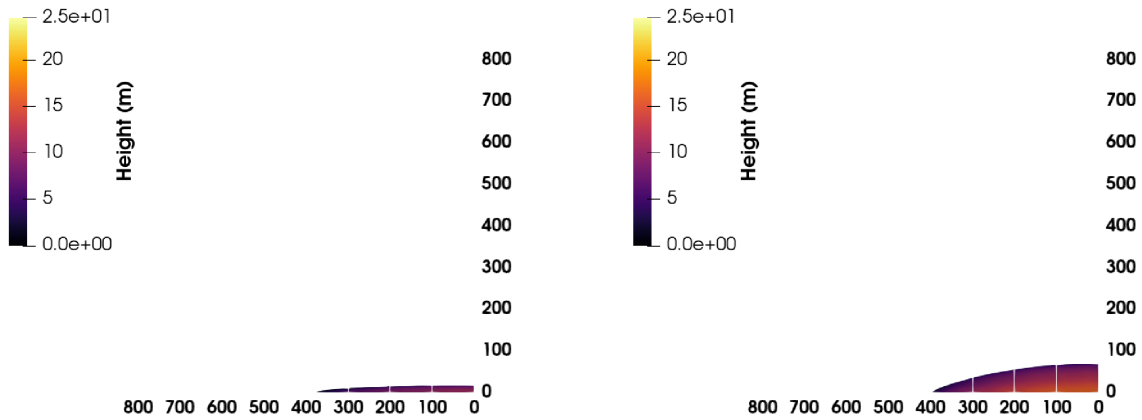

(a) $t = t_Q = 0.02T_s$

(b) $t = 0.1T_s$

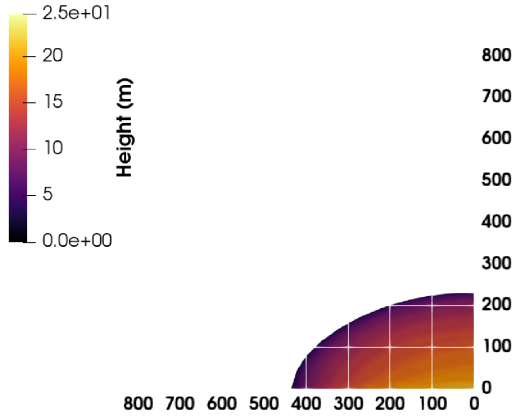

(c) $t = T_s/2$

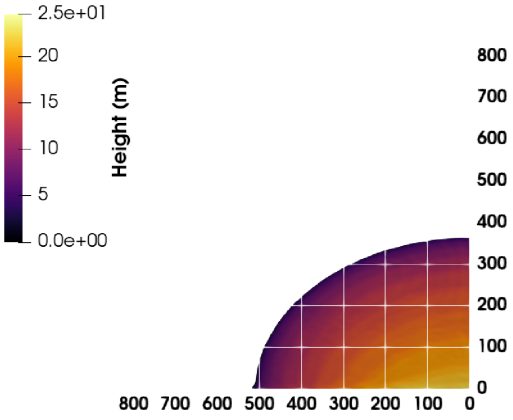

(d) $t = T_s$

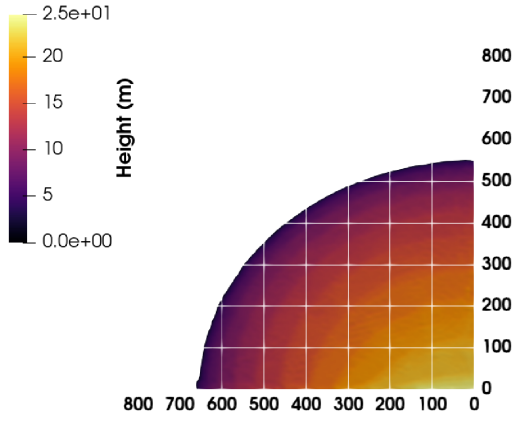

(e) $t = 2T_s$

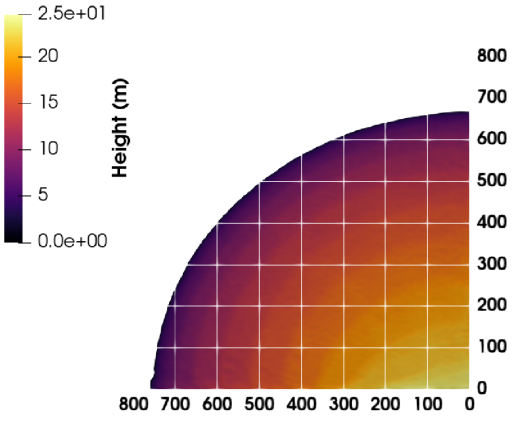

(f) $t = 2.8T_s$

Figure 3. Plan view of the evolution of the dome in simulation V25Q1R0. The vent dimensions $r_x^0 \times r_z^0$ were 400 m × 16 m. We recall that only a quarter of the dome has been simulated based on the symmetry. The view direction is perpendicular to the height y and the colours map the height of the dome (in metre). The horizontal and vertical ticks refer to distances in metre. (For interpretation of the references to colour in this figure legend, the reader is referred to the web version of this paper.)

3.3 Influence of the vent aspect ratio

In simulations V2Q1R1 to V25Q1R0, the aspect ratio of the vent r_x^0/r_z^0 varies between 2 and 25 (see Table 1). Fig. 4 shows the evolution of the growth through the following dimensionless metrics: the height h/H_s, the dome length r_z/r_x^0 along z, the dome length r_x/r_x^0 along x, and the horizontal and transverse aspect ratios of the dome, r_x/r_z and h/r_x and h/r_z, respectively. Three regimes are identified: an initial lava discharge regime with restrained spreading but a mostly linear build-up of the dome height, a subsequent 2-D spreading in the direction perpendicular to the major-axis of the vent and a long-time restored axisymmetric spreading.

As shown in Figs 4(a), (c) and (d), the lava discharge regime occurs in the interval $t/T_s \leq t_Q/T_s$. The duration of the lava-discharge-dominated regime is shorter as the fissure is longer. Simulation V25Q1R0 with vent of aspect ratio $r_x^0/r_z^0 = 25$ is thus characterized by $t_Q/T_s = 0.08$, whereas t_Q/T_s equals 0.2 in simulation V10Q1R0 with vent of aspect ratio $r_x^0/r_z^0 = 10$.

In all simulations with an elliptical vent, except simulations V2Q1R1, V2Q1R0 and V5Q1R00, the lava discharge regime is followed by 2-D spreading in the z direction satisfying $h \propto t^{1/5}$ and $r_z \propto t^{4/5}$ in the interval $t_Q/T_s < t/T_s < 0.5$ (see Figs 4b and c). Between $0.5 < t/T_s < 1.7$, the spreading is found to gradually migrate towards that of an axisymmetric viscous current in both directions x and z, whose spreading rate varies as $t^{1/2}$ (see Figs 4c and d).

In simulations V2Q1R1, V2Q1R0 and V5Q1R00, the vent of aspect ratio characterized by $r_x^0/r_z^0 \leq 5$ cannot be assimilated to a fissure-like vent. Consequently, the lava discharge regime directly changes to the axisymmetric spreading regime in the interval $t_Q/T_s < t/T_s < 1.7$. From $t/T_s > 1.7$, the initial asymmetry of the dome has been reduced to an aspect ratio of the dome that departs from one by 20 per cent in all simulations (Fig. 4e). The initial asymmetry does not decrease below 10 per cent until after $t/T_s > 5$ (Fig. 4e).

Similar to the axisymmetric case, the time at which the lava discharge regime ends is well defined by the maximums of the transverse aspect ratio h/r_z. We also note that h/r_z and h/r_x are generally smaller than one at all times (Fig. 4f). This explains why the similarity solution for the 2-D spreading (eqs 19 and 20) applies at intermediate times. Changes in density (V2Q1R1 and V2Q1R0), volume flux (V10Q1R0 and V10Q10R0) and vent dimensions keeping the same aspect ratio r_x^0/r_z^0 (V10Q1R00 and V10Q1R0) all have metrics that collapse to a single curve in dimensionless space, thus showing the effectiveness of the scaling.

4 DISCUSSION

4.1 Key results

The simulations show that the vent geometry (i.e. the source geometry) has an impact on the spreading of lava domes on a horizontal plane. In this study, we used an elliptic vent whose aspect ratio could vary from 1 to 25, thus covering a range of vents from circular to fissure-like geometries. In the context of sustained lava discharge, the results lead to four main outcomes: (1) lava discharge controls the very early stages of dome growth during which spreading is insignificant and the height of the dome increases at a constant rate over the vent area, (2) provided that the vent is sufficiently elongated, which requires $r_x^0/r_z^0 \geq 5$, subsequent growth is vertical and in the only horizontal direction perpendicular to the elongation of the vent, that is similar to that of a 2-D viscous gravity current, before spreading takes place in the two horizontal directions parallel and perpendicular to the elongation of the vent, (3) long-term spreading behaves as an axisymmetric viscous gravity current and (4) any initial fissure-like geometry of the dome due to that of the vent is bound to diminish over time but to varying degrees. Quantitatively, two timescales, t_Q and T_s characterizing lava discharge and viscous gravity-driven spreading delimit the three regimes and similarity solutions for 2-D and axisymmetric buoyancy-driven viscous currents propagating over a rigid surface apply.

When $t < t_Q$, the height builds up whereas limited spreading occurs. When $t_Q < t < T_s/2$, spreading is in the direction perpendicular to the semi-major axis of the vent at a rate $\propto t^{4/5}$. Between $T_s/2 < t < 1.7T_s$, the growth dynamics changes towards an axisymmetric spreading at a rate $\propto t^{1/2}$. Full axisymmetry of the dome is recovered from $t \geq 5T_s$. In practice, assuming a sustained effusive flux of 1 m^3 s^{-1} and a lava viscosity and density of 10^{11} Pa s and 2300 kg m^{-3} respectively, a dome fed by a fissure of length 100 m and width 5 m would propagate a distance of about 32 m perpendicular to the major axis of the vent in about 2 days. The rate of propagation would then decrease until it matches that of an axisymmetric current. The later regime of propagation would not be expected to start before 7 days. It would take around 20 days before the dome axis symmetry is restored and the dome would have reached a height of $\approx$ 92 m in the first 20 hr. On the other hand, all parameters being equal otherwise, a sustained effusive flux of 10 m^3 s^{-1} would lead to a 2-D propagation of about 32 m in 8 hr 40 min before switching to an axisymmetric propagation, all asymmetry having disappeared after 3.6 days. The dome height would be $\approx$ 163 m.

4.2 Implications

Although the volcanic system is reduced to an isoviscous model as explained in Section 2.1, several outcomes can be drawn from the simulations. First of all, the maximum height of the dome $h(t)$ during a sustained eruption appears to be reasonably well described by the functional that describes the axisymmetric height of the dome $\mathcal{H}(0)$ (eq. 17). When the vent is axisymmetric, there is full agreement. When the vent is elliptic, the height eventually reaches a plateau that is within 9–16 per cent of $\mathcal{H}(0)$. Within this framework, a given dome height H corresponds to possible values of the effusive flux Q and effective viscosity μ_l involved in the dome growth. As shown by Fig. 5, a scan of the surface $H = \mathcal{F}(Q, \mu_l)$, where $\mathcal{F}$ is given by eq. (17) allows to either discard or infer potential candidates (Q, μ_l). For instance, a dome height of 50 m could be associated with pairs (Q, μ_l) that are delimited by the region $Q = [0.1, 7]$ m^3 s^{-1} and $\mu_l = [2.6 \times 10^9, 1.9 \times 10^{11}]$ Pa s. We note that potential candidates could be further constrained by considering the conduit flow dynamics.

Besides, the existence of elongated domes originated from a fissure such as those listed in Table 2 indicates that the lava dome growth terminated before the late axisymmetric stage could be reached. One hypothesis is that the yield strength of the developing crust stopped the growth (Griffiths & Fink 1993; Blake & Bruno 2000; Magnall *et al.* 2017), before radial symmetry could occur. Waning of the effusive flux in a short timescale as it is commonly observed during volcanic eruptions (e.g. Diefenbach *et al.* 2013) would significantly reduce the spreading rate from $t^{4/5}$ to $t^{1/5}$ (Huppert 1982), but it would not halt the flow. Blake & Bruno (2000) proposed a characteristic time for the transition to crust control in

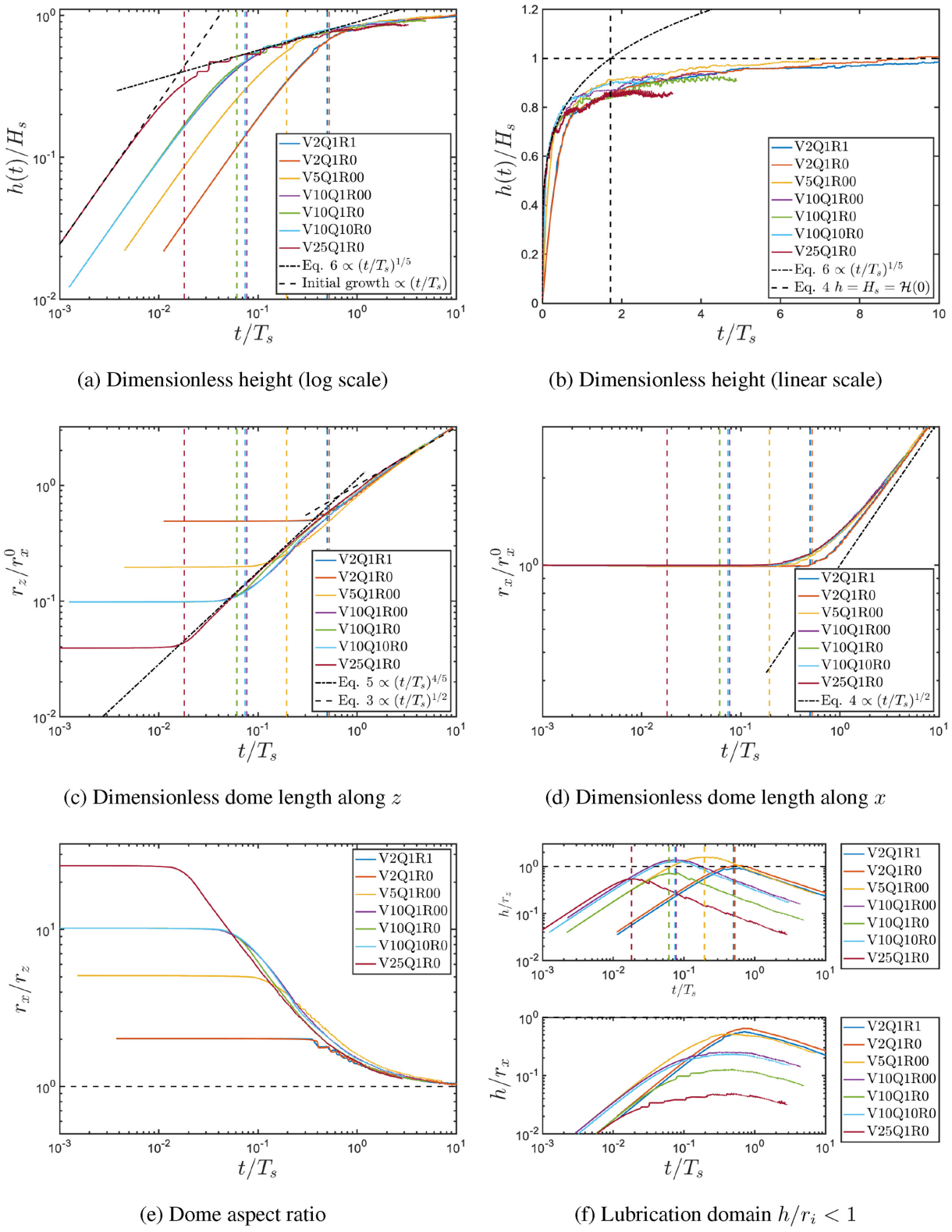

(a) Dimensionless height (log scale)

(b) Dimensionless height (linear scale)

(c) Dimensionless dome length along z

(d) Dimensionless dome length along x

(e) Dome aspect ratio

(f) Lubrication domain $h/r_i < 1$

Figure 4. Dynamics of the dome with elliptical vents at constant lava discharge Q. (a) The coloured dashed lines mark the limit of the lava discharge regime $t/T_s = t_Q/T_s$ as defined in Section 2.3. (b) The vertical black dashed line indicates the end of the 2-D spreading $t_{2d\rightarrow 3d}$, time which will be introduced in Section 4.2. The dashed black line in (a) corresponds to the $h(t)/H_s = 2QT_s/[\pi r_x^0 r_z^0](t/T_s)$. (For interpretation of the references to colour in this figure legend, the reader is referred to the web version of this paper.)

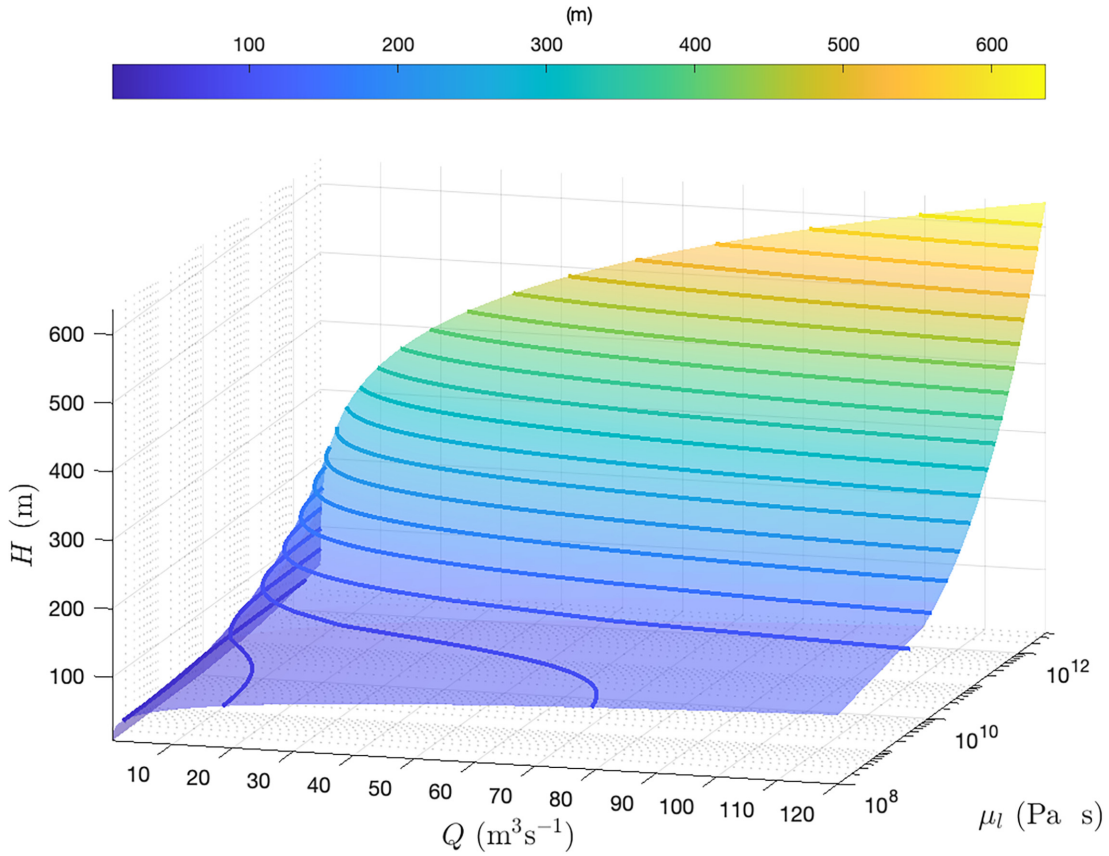

Figure 5. 3-D surface and isolines every 20 m of $\mathcal{H}(0)$ as a function of Q and μ_l. The range of Q is based on the compilation by fig. 11 of Pallister *et al.* (2013) with a maximum of 120 m^3 s^{-1}. We note that very large effusive flow rate is usually short-lived. The range of effective viscosity was chosen as [10^8, 4 $\times$ 10^{12}] Pa s. Pairs (Q, μ_l) cover the range observed for heights of lava domes since the tallest lava dome, Lassen Peak, reached 600 m. (For interpretation of the references to colour in this figure legend, the reader is referred to the web version of this paper.)

Table 2. Documented lava dome eruptions from a fissure vent. Dimensions are respectively given along the x, y and z axes. Lengths of the fissure was inferred either at depth or at the surface, in which case it is kilometric and not systematically representing the vent extent.

Dome	Region	Date	Dimensions	r_x/r_z	L_f	References
Taylor Creek Rhyolite Domes	New Mexico, USA	27.9 Ma	7.6 km× 60 m × 3.7 km (Tt7)	2.0	>30 km	Duffield *et al.* (1995)
			9 km×? m × 4.5 km (Tt2)	2.0	>30 km	
Douglas Knob	Yellowstone, USA	116 ka	670 m× 32 m × 470 m	1.4	500 m	Christiansen *et al.* (2007)
						Befus *et al.* (2014)
Puketerata Volcanic Domes	Central Taupo Volcanic zone, NZ	14 ka	300 m× 75 m × 200 m	1.5	2.5 km	Kósik *et al.* (2019)
			825 m × 115 m × 580 m	1.2	200 m	Kósik *et al.* (2019)
South Coulee	Mono-Inyo Craters, USA	0.6 ka	3.6 km × 75 m × 1.2 km	3	>3.8 km	Loney (1968)
						Leggett *et al.* (2020)
Panum Dome	Mono-Inyo Craters, USA	0.7 ka	–	–	700 m	Sieh & Bursik (1986)
Obsidian Dome	Mono-Inyo Craters, USA	0.55-0.65 ka	1.8 km× 100 m × 1.5 km	1.2	–	Miller (1985); Kingsbury (2012)
						Vogel *et al.* (1989); Swanson *et al.* (1989)
Showa Iwo-jima	Southern Kyushu, Japan	1935	530 m× 55 m × 270 m	2.0	–	Maeno & Taniguchi (2006)
Cordón Caulle Volcanic Complex	Southern Andes, Chile	1960	–	–	5 km	Lara *et al.* (2004)
Mount St. Helens	Cascades, USA	1980	–	–	–	Waite *et al.* (2008)
		2007				
Santiaguito Dome Complex	Southwest, Guatemala	2009	–	–	50 m	Forbes (2010)
Fuego de Colima	Colima, Mexico	2013	160 m×? m × 100 m	1.4	–	Zorn *et al.* (2019)
		2015	195 m×? m × 110 m	1.8	–	Zorn *et al.* (2019)

the case of a line source as follows:

$$t_C = \left(\frac{(\rho_l^3 g^3 \mu_l^2 q^4)^{1/5}}{\sigma \kappa^{1/2}} \right)^{10}, \tag{22}$$

where σ is the yield stress (strength) and κ is the thermal diffusivity. The time t_C is actually poorly constrained by eq. (22) because large values of the exponents describe its dependence on Q, μ_l and σ, which are unknowns. Nevertheless, if we assume that the transition likely occurs in the interval $T_s \leq t_C < 5T_s$, we can infer bounds for the strength σ. Taking a fissure vent of length $2r_x^0 = 200$ m, an effusive flow rate $Q = 10$ m^3 s^{-1} and a lava density and viscosity $\rho_l = 2300$ kg m^{-3} and $\mu_l = 3 \times 10^5$ Pa s, the condition $T_s \leq t_C < 5T_s$ implies that 3.97×10^6 Pa $\leq \sigma < 4.66 \times 10^6$ Pa. Such a range falls in the range of values previously estimated by Griffiths & Fink

(1993) and Blake & Bruno (2000), that is $[10^4 - 1.3 \times 10^8]$ Pa. It is therefore plausible that some domes issued from a fissure remained elliptical in shape following a transition from the viscous regime to the crust-dominated regime.

In our simulations, the influence of the pressure gradient due to the lava discharge was negligible compared to that of gravity, we thus satisfied $t_B \ll t_Q$ or $\mu_l/(\rho_l g \mathcal{H}(0)) \ll \pi \mathcal{H}(0)(r_x^0)^2/Q$ for a circular vent and $\mu_l/(\rho_l g H_{2d}) \ll H_{2d} r_z^0/q$ for an elliptical vent. These conditions may be rearranged and viewed as a function of Q, giving a limit Q_l above which the lava discharge would dominate over gravity at all times. The limit Q_l is given by

$$Q_l = 1.2794^4 \pi^2 \frac{3\rho_l g}{\mu_l} (r_x^0)^4 \tag{23}$$

for the circular vent and

$$Q_l = 1.325^8 3^2 \frac{\rho_l g r_x^0 (r_z^0)^3}{\mu_l} \tag{24}$$

for the elliptical vent. In the case where the lava density and viscosity would be 2300 kg m^{-3} and 10^{11} Pa s respectively, the limit Q_l would be 112 m^3 s^{-1} when the dome is fed by a circular vent of radius 50 m and 0.8 m^3 s^{-1} when the dome is fed by a fissure of length 200 m and width 15 m. So a lava discharge dominated regime cannot be discarded in some cases of dome growth and it would be more likely when the vent is a fissure.

Last but not least, as shown by our simulations, the evolution of the dome largely depends on the fissure length, a dimension that is either unknown or hard to infer in the field. In this context, our simulations and eqs (17), (19) and (20) can provide a hint on the fissure length. If we assume that the height of the dome $\mathcal{H}_{2d}(0, t)$ evolves as in the 2-D propagation (eq. 20) until it reaches the constant height $\mathcal{H}(0)$ (eq. 17), the time of transition $t_{2d\to 3d}$ is given by

$$t_{2d\to 3d} \approx 4 \left(\frac{1.2794}{1.325}\right)^5 \left(\frac{3\mu_l}{\rho_l g Q^3}\right)^{1/4} (r_x^0)^2, \tag{25}$$

which is equivalent to the dimensionless time $t_{2d\to 3d}/T_s = 1.7$. According to our simulations, the aspect ratio of the dome at that time is 1.2–1.3. Following eq. (19), the front $\mathcal{Z}_n(t_{2d\to 3d})$ is also related to the fissure length r_x^0 by

$$\mathcal{Z}_n(t_{2d\to 3d}) = 2 \left(\frac{1.2794}{1.325}\right)^4 r_x^0 = 1.7386 r_x^0. \tag{26}$$

Hence, an elliptic dome of length r_z and aspect ratio r_x/r_z around $1.2 - 1.3$ would have originated from a vent of semi-major axis $r_x^0 = r_z/1.7386$.

Eq. (25) is approximate because the height of the dome $\mathcal{H}_{2d}(0, t_{2d\to 3d})$ differs from $\mathcal{H}(0)$ by 9–16 per cent in our simulations. This introduces a discrepancy in $t_{2d\to 3d}$ of order $\delta t/t \approx [(1 + \delta h/h)^5 - 1]$, and a correction by a factor of 0.38–0.58 (see Fig. 4b). This inaccuracy in $t_{2d\to 3d}$ ultimately leads to an overestimate of the vent half-length by a factor $(1 + \delta t/t)^{4/5}$, that is a correction factor of 1.29–1.44. Accessing an upper bound range for the fissure vent length seems nevertheless useful. We note that the applicability of eq. (26) requires that the aspect ratio of the dome r_x/r_z is less than 1.5 because when $r_x/r_z \geq 1.5$ ($t/T_s < 1$), the height of the dome $\mathcal{H}_{2d}(0, t)$ has not reached its plateau and a value within 9–16 per cent of $\mathcal{H}(0)$ (see also Fig. 4b). So the assumption leading to eq. (25) no longer makes sense.

In the case where a fossil dome has an aspect ratio $r_x/r_z \approx 1.2 - 1.3$, eqs (25) and (26) may be used to infer an estimate of the fissure length and the duration of lava discharge. The key consideration behind this undertaking is that the lava discharge could not have occurred during a time T_f exceeding the time $t_{2d\to 3d}$ because a time T_f such that $T_f > t_{2d\to 3d}$ would actually have led to an aspect ratio of the dome lower than 1.2–1.3. So, $t_{2d\to 3d}$ represents the upper limit for the duration of lava discharge. We note that it is possible that the lava discharge stopped somewhat before the dome had reached the aspect ratio of 1.2–1.3 but without $T_f \ll t_{2d\to 3d}$. Otherwise, the aspect ratio of 1.2–1.3 may not have been reached before cooling prevailed. This is because the evolution of the dome after the lava discharge ceases is much slowed down with the rate of propagation dropping by a factor 4, that is the difference in propagation rate between a propagation at constant volume flux and a propagation at constant volume (Huppert 1982). So, it seems reasonable to assume that T_f was not so different from to $t_{2d\to 3d}$. Furthermore, given the fossil volume of the dome V_{obs}, frozen at the time T_f of lava discharge cessation,

$$V_{obs} = Q T_f \sim Q t_{2d\to 3d}, \tag{27}$$

which leads to

$$\frac{V_{obs}}{Q} \approx 1.7 T_s \tag{28}$$

with

$$Q \approx \left[\frac{V_{obs}}{1.7\left(\frac{r_x^0}{0.715}\right)^2}\right]^4 \left(\frac{\rho_l g}{3\mu_l}\right). \tag{29}$$

4.3 Natural terrestrial examples

Elongated lava domes or coulees issued from a fissure vent similar to those listed in Table 2 all presented evidence of flow perpendicular to the direction of the main fissure or fissure vent. For instance, Sieh & Bursik (1986) describe the Panum North dome as having an elliptical shape in north-south plan from which lava exited after a corner flow, the north-south 'diameter' of the dome being shorter. South Coulee of the Mono-Inyo range erupted from a north–south trending fissure whereas the flow spread both east and west from the fissure (Loney 1968; Leggett *et al.* 2020). The 2-D propagation perpendicular to the semi-major axis of the vent documented in this study thus agrees with the observations.

4.3.1 Obsidian Dome, Mono-Inyo Craters, USA

The Obsidian dome is an asymmetric extrusion of high silica rhyolite situated along the 11-km-long Inyo volcanic chain in eastern California (see Table 2). The dome is part of a series of eruptive vents aligned along north-trending fissures. A feeder dyke at shallow depths is believed to have fed the dome (Vogel *et al.* 1989). Although research drilling in the Obsidian dome did two drill holes in the dome, and two drill holes near it to sample the dyke at depth, the vent geometry was not probed (Eichelberger *et al.* 1984; Swanson *et al.* 1989). Yet, the dome is not circular, which suggests that the vent was elliptical. The dimensions of the dome are 1.8 km × 100 m × 1.5 km (Vogel *et al.* 1989; Kingsbury 2012) with an estimated volume of 0.17 km^3 (Miller 1985). The aspect ratio of the dome of 1.2 allows the application of eq. (26). Assuming $\mathcal{Z}_n(t_s) = 1500/2$ m, $r_x^0 = 430$ m, implying that an upper bound for the vent length is 860 m. Besides, assuming a volume of the dome $V_{obs} = 0.17$ km^3, a density $\rho_l = 2300$ kg m^{-3} and an effective lava viscosity $\mu_l = 10^{12}$ Pa s, a value chosen close to the viscosity of the crust of $10^{12.8}$ Pa s given by Leggett *et al.* (2020) based on Lister

& Kerr (1994), eqs (28) and (29) predict that a volume flux of lava of 42.8 m^3 s^{-1} would have fed the dome and that the lava discharge would have lasted 46 days. These estimates are comparable to the volume flux of 60 m^3 s^{-1} and the emplacement time of 30 days derived by Leggett *et al.* (2020) assuming axisymmetric spreading at constant volume release, a propagation regime which may not be the most suitable to represent the growth of the dome.

4.3.2 Douglas Knob, Yellowstone volcanic field, USA

Douglas Knob is a lava dome that is part of the Yellowstone volcanic system. The dome of volume 0.01 km^3 forms an ellipsoidal mound ∼700 m long, ∼32 m thick and ∼500 m wide (Christiansen *et al.* 2007; Befus *et al.* 2014). It was proposed to have erupted from a 500-m-long fissure instead of a central vent (Befus *et al.* 2014). The fissure length was loosely constrained by these latter authors to allow reasonable eruption rates assuming that the length of the fissure vent was the same as the fissure at depth. With the aspect ratio of the dome of 1.4 still in a reasonable range of application of eq. (26), the upper bound for the estimate of the length of the fissure vent is 288 m, a length that is somewhat shorter than the value proposed by Befus *et al.* (2014). Besides, assuming a volume of the dome $V_{obs} = 0.01$ km^3, a density $\rho_l = 2300$ kg m^{-3}, and an effective lava viscosity $\mu_l = 10^{12}$ Pa s, a value also inferred by Befus *et al.* (2014), which relates to a temperature of magma of 760°C prior to eruption and a low content of phenocrysts (5 per cent), eqs (28) and (29) predict that a volume flux of lava of 3.3 m^3 s^{-1} would have fed the dome and that the lava discharge would have lasted 34 days. Such a duration of discharge is six times shorter than the estimate by Befus *et al.* (2014) at 210 days again based on an equation for the axisymmetric spreading of a current at constant volume release, where the runout length slowly varies as $t^{1/8}$.

4.3.3 Puketerata volcanic larger dome, Central Taupo volcanic zone, NZ

The Puketerata volcanic complex have been associated with a 2.5 km long NE- trending eruptive fissure (Kósik *et al.* 2019). The asymmetry of the lava domes has not entirely been erased (see Table 2). The largest of the two domes of volume 0.0505 km^3 has an aspect ratio of 1.2 with dimensions 825 m × 115 m × 580 m (Kósik *et al.* 2019). These dimensions include buried parts of the dome estimated at ≈50–100 m. Hence they differ from an earlier study by Brooker *et al.* (1993) who gave 560 m × 80 m × 450 m. If we nevertheless assume that $\mathcal{Z}_n(t_s) = 580/2$ m, eq. (26) leads to $r_x^0 = 167$ m, a value which would *a priori* be an overestimate of the vent fissure half-length by a factor of about 1.3–1.4. A corrected r_x^0 would thus be 119–128 m, implying a vent of length 238–257 m. This value is in reasonable agreement with the study of Kósik *et al.* (2019) suggesting a 200-m-long fissure vent (see Table 2). Kósik *et al.* (2019) and Brooker *et al.* (1993) further report a relatively low eruption temperature of 750 °C and a high content of phenocrysts (16–20 per cent), which points to a value of the effective viscosity that would have been higher than 10^{11} Pa s. The trend proposed in fig. 4 of Di Genova *et al.* (2017) for the rheological agpaitic index further supports a variation of the viscosity between these three domes following $\mu_l^{\text{Inyo}} < \mu_l^{\text{Douglas}} < \mu_l^{\text{Taupo}}$. However, if we assume a volume of the dome $V_{obs} = 0.0505$ km^3, an effective lava viscosity $\mu_l = 10^{12}$ Pa s and a density $\rho_l = 2300$ kg m^{-3}, eqs (28) and (29) predict that a volume flux of lava of 665 m^3 s^{-1} would have fed the dome and that the lava discharge would have lasted 21 hr. Such a very high flux does not appear to be a reasonable estimate, especially given the high 73 per cent SiO_2 content of the Puketerata magma (Yokoyama 2005; Kósik *et al.* 2019). This suggests that the dome did not result from a single continuously fed eruptive event, but rather multiple episodes.

4.4 Lava domes on Venus

The existence of lava domes on Venus has been recognized since the NASA's Magellan mission. The vast majority of domes are steep-sided and have a pancake shape with diameters up to 100 km and volumes in the range 25–3400 km^3 (Guest *et al.* 1992; McKenzie *et al.* 1992; Pavri *et al.* 1992). Compared to the Earth, these domes appear significantly larger. Only the 10–200 km^3 volume range reported for the rhyolitic lava flows in the Snake River Plain, Idaho may be comparable (Pavri *et al.* 1992). The mechanism of emplacement is attributed to steady high effusion rate events leaving insufficient time for cooling (Pavri *et al.* 1992). Axisymmetric viscous gravity-driven currents thus well describe lava dome eruptions (McKenzie *et al.* 1992; Quick *et al.* 2016).

Furthermore, there is clear evidence of the presence of extensional features, such as rift valleys and grabens, and dykes and fissural systems in the plains surrounding domes suggesting an interrelationship (Ernst *et al.* 1995; Guseva & Ivanov 2019). Similar to many terrestrial counterparts, lava domes on Venus occurred in cluster parallel to the lineaments. Although Pavri *et al.* (1992) suggested that andesitic to rhyolitic magma on Venus could have erupted through fissures, the idea of domes grown from fissure vents was seemingly not proposed because it was not compatible with the observed radial symmetry of the domes.

This study actually allows to revisit the latter concept since a dome fed sustainably from a fissure vent and not prone to cooling, conditions presumably fulfilled on Venus, can attain radial symmetry in a characteristic time $t \approx 5T_s$. A realistic condition for the duration of lava discharge T_f would thus be a time window around $t = 5T_s$. Using $T_f = 5T_s$ as a baseline for the duration of lava discharge and considering that the fossil diameter of the dome, D_{obs}, would not differ much from its value at the time of cessation of lava discharge, that is $D_{obs} \approx 2\mathcal{R}_n(T_f)$, which is reasonable because the spreading rate is significantly reduced once the lava discharge stops, eqs (17) and (21) lead to a fissure length given by

$$2r_x^0 \approx \frac{D_{obs}}{\sqrt{5}}. \tag{30}$$

A dome of diameter 28.8 km (i.e. mode diameter calculated from Pavri *et al.* 1992) could thus not have emerged from a fissure vent exceeding a length of 13 km.

Given the presumed conditions of emplacement (high and sustained Q, no cooling effect), another reasonable assumption is to consider that the maximum height of the dome given by eq. (18) was reached during the eruption. In this context, if we combine eqs (18) and (21), we can eliminate the effective viscosity, which gives the relation

$$\mathcal{H}(0) = 5 \times 1.60 \times (0.715)^{8/3} \frac{QT_s}{(r_x^0)^2}. \tag{31}$$

Fig. 6 shows isosurfaces of the dome height $\mathcal{H}(0)$ given by eq. (31) as a function of (r_x^0, Q, T_s). As shown in Fig. 6, eruptions most likely occurred within tens of years. The radial dimension and the volume of the dome have however not explicitly been used as a constraint.

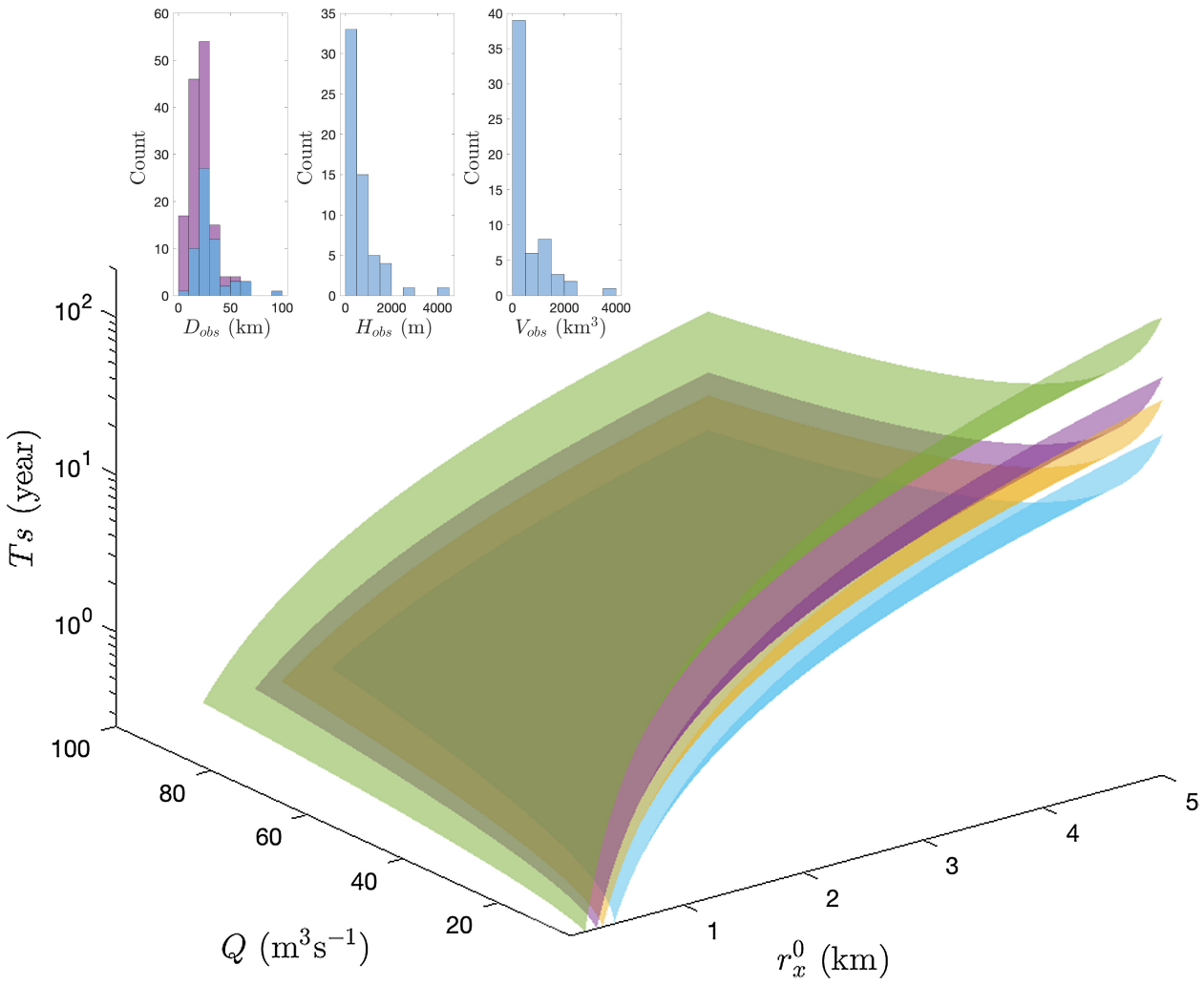

Figure 6. Isosurfaces $\mathcal{H}(0)$ at heights 250, 750, 1250, 1750 and 3500 m (stacked from bottom to top) as a function of (r_x^0, Q, T_s). The inset shows histograms of all the measured dome heights, diameters and volumes, respectively, H_{obs}, D_{obs} and V_{obs}, given in table 1 of Pavri *et al.* (1992). Note that heights and volumes were not systematically measured unlike diameters. Two histograms based on all diameters (in blue) and diameters associated with heights (in red) are thus shown. The maximum of r_x^0 has been chosen as 5 km, which corresponds to the median value $(D_{obs})/(2\sqrt{5})$. (For interpretation of the references to colour in this figure legend, the reader is referred to the web version of this paper.)

Given eqs (30) and (31) can be further rearranged to give an estimate of the duration of lava discharge as follows:

$$T_f \approx \frac{H_{obs} D_{obs}^2}{13Q}, \tag{32}$$

where $\mathcal{H}(0)$ has been taken as equal to the height of the fossil dome, H_{obs}. Eq. (32) is actually equivalent to the direct relation between the volume of the dome V_{obs} and the volume flux Q, $T_f = V_{obs}/Q$, since V_{obs} is expected to scale as $H_{obs} D_{obs}^2$ times a geometrical factor depending on the shape of the dome. A correction factor (>1) would be needed in eq. (32) if $H_{obs} \leq \mathcal{H}(0)$.

If we use the modes for the dome height and diameter calculated from Pavri *et al.* (1992) based on the measured pairs (H, D), $H_{obs} = 193$ m and $D_{obs} = 28.8$ km, and assume a sustained volume flux of $Q = 50$ m^3 s^{-1}, the duration of lava discharge would last within 7.8 yr according to eq. (32). We have chosen the mode as metric here because the two diameter distributions in the inset of Fig. 5 suggest that smaller diameters are underrepresented in the distribution sampling the pairs (H, D) and therefore the peak of the actual height distribution at low heights could be even higher. Alternatively, using $V_{obs} = 220$ km^3, the mode of the volume distribution estimated by Pavri *et al.* (1992) (see inset of Fig. 6) and $Q = 50$ m^3 s^{-1}, the eruption would last within 140 yr. The direct estimate of the duration of discharge based on the measured volume appears longer but it may be necessary to keep in mind that the dome volume measurements were not very well constrained (Pavri *et al.* 1992).

4.5 Conclusion

The robust numerical simulations of this study made it possible to show the importance of the geometry of the vent on lava domes and the variety of the growth regimes. The aspect ratio of the vent (i.e. the ratio of the semi-major axis to the semi-minor axis of the vent) clearly determines the evolution of the eruption. In the case of sustained eruptions, the dome growth evolves in two or three main phases depending on the aspect ratio of the vent. When the ratio is two, the growth is first vertical with insignificant horizontal spreading and then radial with swelling of the dome from a maximum height. When the ratio is five and above, a vertical growth

associated with spreading perpendicular to the semi-major axis of the vent is inserted between the two previous phases. A lava dome sustainably fed by a fissure vent eventually becomes circular, erasing the signature of the vent geometry. We characterized two times to delimit the different phases, a time linked to the dominance of lava discharge and a time linked to the dominance of gravity, both depending on the dimensions of the vent. We show that similarity solutions apply. In particular, the spreading perpendicular to the semi-major axis of the vent is well described by the viscous propagation of a 2-D buoyancy-driven gravity current. When applied to natural lava domes, this study provides relationships to estimate the length of fissure vents, a dimension which is not accessible by any direct observations, and the duration of discharge according to the shape of fossil domes. These relations, which are constrained by the dome aspect ratio and the growth rate associated with it, are applied to three asymmetric terrestrial domes and the circular domes on Venus. We hope that this study will be useful to the community and provide an additional incentive for further monitoring of the growth of lava domes.

ACKNOWLEDGMENTS

The numerical work was supported by computational resources provided by the Monash eResearch Centre and eSolutions-Research Support Services through the use of the MonARCH HPC Cluster. C.M. warmly thanks Simon Michnowicz from Monash eResearch Centre and Professors Peter Betts and Andrew Mackintosh from the School of Earth, Atmosphere and Environment for their support during this work. Thoughtful reviews and comments from Editor Gaël Choblet, Oleg Melnik and Alik Ismail-Zadeh are gratefully acknowledged.

DATA AVAILABILITY

The parallel particle-in-cell finite element code *ptatin3d* is an open source software available at https://bitbucket.org/ptatin/ptatin3d. The data underlying this paper will be shared on reasonable request to the corresponding author.

REFERENCES

Aguirre-Díaz, G.J. & Labarthe-Hernández, G., 2003. Fissure ignimbrites: fissure-source origin for voluminous ignimbrites of the Sierra Madre Occidental and its relationship with basin and range faulting, *Geology,* **31**(9), 773–776.

Balay, S., Gropp, W.D., McInnes, L.C. & Smith, B.F., 1997. Efficient management of parallelism in object oriented numerical software libraries, in *Modern Software Tools in Scientific Computing,* pp. 163–202, eds Arge, E., Bruaset, A.M. & Langtangen, H.P., Birkhäuser Press.

Balay, S. *et al.*, 2017. *PETSc Users Manual, ANL-95/11—Revision 3.8,* Argonne National Laboratory.

S., Balay *et al.*, 2022. *PETSc Web page*. Available at: https://petsc.org/.

Befus, K.S., Zinke, R.W., Jordan, J.S., Manga, M. & Gardner, J.E., 2014. Pre-eruptive storage conditions and eruption dynamics of a small rhyolite dome: Douglas Knob, Yellowstone volcanic field, USA, *Bull. Volcanol.,* **76**(3), 1–12.

Blake, S. & Bruno, B., 2000. Modelling the emplacement of compound lava flows, *Earth planet. Sci. Lett.,* **184**(1), 181–197.

Brooker, M., Houghton, B., Wilson, C. & Gamble, J., 1993. Pyroclastic phases of a rhyolitic dome-building eruption: Puketarata tuff ring, tAupo Volcanic Zone, New Zealand, *Bull. Volcanol.,* **55**(6), 395–406.

Christiansen, R.L. *et al.*, 2007. Preliminary assessment of volcanic and hydrothermal hazards in Yellowstone National Park and vicinity. Open-File Rep, U.S. Geol. Surv., 2007-1071.

Costa, A., Melnik, O. & Sparks, R., 2007. Controls of conduit geometry and wallrock elasticity on lava dome eruptions, *Earth planet. Sci. Lett.,* **260**(1–2), 137–151.

Crameri, F. *et al.*, 2012. A comparison of numerical surface topography calculations in geodynamic modelling: an evaluation of the "sticky air" method, *Geophys. J. Int.,* **189**(1), 38–54.

Diefenbach, A.K., Bull, K.F., Wessels, R.L. & McGimsey, R.G., 2013. Photogrammetric monitoring of lava dome growth during the 2009 eruption of Redoubt Volcano, *J. Volc. Geotherm. Res.,* **259,** 308–316.

Di Genova, D., Kolzenburg, S., Wiesmaier, S., Dallanave, E., Neuville, D.R., Hess, K.-U. & Dingwell, D.B., 2017. A compositional tipping point governing the mobilization and eruption style of rhyolitic magma, *Nature,* **552**(7684), 235–238.

Duffield, W.A., Richter, D.H. & Priest, S.S., 1995. Physical volcanology of silicic lava domes as exemplified by the Taylor Creek Rhyolite, Catron and Sierra counties, New Mexico. U.S. Geol. Surv. Map I-2399, 1:50,000, pp. 1-16.

Eichelberger, J.C., Lysne, P.C. & Younker, L.W., 1984. Research drilling at Inyo domes, Long Valley caldera, California, *EOS, Trans. Am. geophys. Un.,* **65**(39), 721–725.

Ernst, R., Head, J., Parfitt, E., Grosfils, E. & Wilson, L., 1995. Giant radiating dyke swarms on Earth and Venus, *Earth Sci. Rev.,* **39**(1–2), 1–58.

Fink, J.H. & Anderson, S.W., 2000. Lava domes and coulees, in *Encyclopedia of Volcanoes,* pp. 307–319, ed. Sigurdsson, H., Academic Press.

Fink, J.H. & Griffiths, R.W., 1992. A laboratory analog study of the surface morphology of lava flows extruded from point and line sources, *J. Volc. Geotherm. Res.,* **54**(1–2), 19–32.

Fink, J.H. & Griffiths, R.W., 1998. Morphology, eruption rates, and rheology of lava domes: insights from laboratory models, *J. geophys. Res.,* **103**(B1), 527–545.

Fink, J.H. & Pollard, D.D., 1983. Structural evidence for dikes beneath silicic domes, Medicine Lake Highland Volcano, California, *Geology,* **11**(8), 458–461.

Forbes, C.C., 2010. Surficial behavior of lava extruded by Santiaguito Dome, Guatemala, during January 2007 and January 2009, *PhD thesis*, New Mexico Institute of Mining and Technology.

Griffiths, R.W. & Fink, J.H., 1993. Effects of surface cooling on the spreading of lava flows and domes, *J. Fluid Mech.,* **252,** 667–702.

Guest, J.E. *et al.*, 1992. Small volcanic edifices and volcanism in the plains of Venus, *J. geophys. Res.,* **97**(E10), 15 949–15 966.

Guseva, E. & Ivanov, M., 2019. Regional geologic and morphologic characterization of rift zones on Venus, *Sol. Syst. Res.,* **53**(4), 233–244.

Hale, A.J., Bourgouin, L. & Mühlhaus, H., 2007. Using the level set method to model endogenous lava dome growth, *J. geophys. Res.,* **112**(B3), doi:10.1029/2006JB004445.

Huppert, H.E., 1982. The propagation of two-dimensional and axisymmetric viscous gravity currents over a rigid horizontal surface, *J. Fluid Mech.,* **121,** 43–58.

Huppert, H.E., Shepherd, J.B., Sigurdsson, R.H. & Sparks, S.J., 1982. On lava dome growth, with application to the 1979 lava extrusion of the soufriere of St. Vincent, *J. Volc. Geotherm. Res.,* **14**(3–4), 199–222.

Jaupart, C., 1991. Effects of compressibility on the flow of lava, *Bull. Volcanol.,* **54**(1), 1–9.

Jones, T.J. & Llewellin, E.W., 2021. Convective tipping point initiates localization of basaltic fissure eruptions, *Earth planet. Sci. Lett.,* **553,** 116637.

Kaneko, T., Wooster, M.J. & Nakada, S., 2002. Exogenous and endogenous growth of the Unzen lava dome examined by satellite infrared image analysis, *J. Volc. Geotherm. Res.,* **116**(1–2), 151–160.

Kingsbury, C.G., 2012. Physical volcanology of Obsidian Dome, California: a complex record of emplacement of a youthful lava dome, *PhD thesis*, University of Ottawa.

Kósik, S., Németh, K., Lexa, J. & Procter, J., 2019. Understanding the evolution of a small-volume silicic fissure eruption: Puketerata volcanic complex, Taupo Volcanic Zone, New Zealand, *J. Volc. Geotherm. Res.,* **383,** 28–46.

Lara, L., Naranjo, J. & Moreno, H., 2004. Rhyodacitic fissure eruption in Southern Andes (CordóN Caulle; 40.5 s) after the 1960 (M_w: 9.5) Chilean

earthquake: a structural interpretation, *J. Volc. Geotherm. Res.,* **138**(1–2), 127–138.

Leggett, T.N., Befus, K.S. & Kenderes, S.M., 2020. Rhyolite lava emplacement dynamics inferred from surface morphology, *J. Volc. Geotherm. Res.,* **395,** 106850.

Lister, J.R. & Kerr, R.C., 1989. The propagation of two-dimensional and axisymmetric viscous gravity currents at a fluid interface, *J. Fluid Mech.,* **203,** 215–249.

Lister, J.R. & Kerr, R.C., 1994. Influence of cooling on lava-flow dynamics: comment and reply, *Geology,* **22**(1), 93–94.

Loney, R.A., 1968. Flow structure and composition of the Southern Coulee, Mono Craters, California–a pumiceous rhyolite flow, in *Studies in Volcanology,* Vol. 116, eds Coats, R.R., Hay, R.L. & Anderson, C.A., Geological Society of America.

Lyman, A.W., Koenig, E. & Fink, J.H., 2004. Predicting yield strengths and effusion rates of lava domes from morphology and underlying topography, *J. Volc. Geotherm. Res.,* **129**(1–3), 125–138.

Maeno, F. & Taniguchi, H., 2006. Silicic lava dome growth in the 1934–1935 Showa Iwo-jima eruption, Kikai caldera, south of Kyushu, Japan, *Bull. Volcanol.,* **68**(7), 673–688.

Magnall, N., James, M.R., Tuffen, H. & Vye-Brown, C., 2017. Emplacing a cooling-limited rhyolite lava flow: similarities with basaltic lava flows, *Front. Earth Sci.,* **5,** 44, doi:10.3389/feart.2017.00044.

May, D.A., Brown, J. & Le Pourhiet, L., 2014. pTatin3D: high-performance methods for long-term lithospheric dynamics, in *SC'14: Proceedings of the International Conference for High Performance Computing, Networking, Storage and Analysis,* New Orleans, LA, USA, pp. 274–284, IEEE.

May, D.A., Brown, J. & Le Pourhiet, L., 2015. A scalable, matrix-free multigrid preconditioner for finite element discretizations of heterogeneous Stokes flow, *Comput. Methods Appl. Mech. Eng.,* **290,** 496–523.

McKenzie, D., Ford, P.G., Liu, F. & Pettengill, G.H., 1992. Pancakelike domes on Venus, *J. geophys. Res.,* **97**(E10), 15 967–15 976.

Miller, C.D., 1985. Holocene eruptions at the Inyo volcanic chain, California: implications for possible eruptions in Long Valley caldera, *Geology,* **13**(1), 14–17.

Pallister, J.S., Diefenbach, A.K., Burton, W.C., Muñoz, J., Griswold, J.P., Lara, L.E., Lowenstern, J.B. & Valenzuela, C.E., 2013. The Chaitén rhyolite lava dome: eruption sequence, lava dome volumes, rapid effusion rates and source of the rhyolite magma, *Andean Geol.,* **40**(2), 277–294.

Pavri, B., Head, J.W., Klose, K.B. & Wilson, L., 1992. Steep-sided domes on Venus: characteristics, geologic setting, and eruption conditions from Magellan data, *J. geophys. Res.,* **97**(E8), 13 445–13 478.

Quick, L.C., Glaze, L.S., Baloga, S.M. & Stofan, E.R., 2016. New approaches to inferences for steep-sided domes on venus, *J. Volc. Geotherm. Res.,* **319,** 93–105.

Rhodes, E., Kennedy, B.M., Lavallée, Y., Hornby, A., Edwards, M. & Chigna, G., 2018. Textural insights into the evolving lava dome cycles at Santiaguito lava dome, Guatemala, *Front. Earth Sci.,* **6,** 30, doi:10.3389/feart.2018.00030.

Sieh, K. & Bursik, M., 1986. Most recent eruption of the Mono Craters, eastern central California, *J. geophys. Res.,* **91**(B12), 12539–12571.

Stasiuk, M.V., Jaupart, C., Stephen, R. & Sparks, J., 1993. Influence of cooling on lava-flow dynamics, *Geology,* **21**(4), 335–338.

Swanson, S.E., Naney, M.T., Westrich, H. & Eichelberger, J., 1989. Crystallization history of obsidian dome, Inyo domes, California, *Bull. Volcanol.,* **51**(3), 161–176.

Tsepelev, I., Ismail-Zadeh, A. & Melnik, O., 2020. Lava dome morphology inferred from numerical modelling, *Geophys. J. Int.,* **223**(3), 1597–1609.

Vogel, T.A., Eichelberger, J.C., Younker, L.W., Schuraytz, B.C., Horkowitz, J.P., Stockman, H.W. & Westrich, H.R., 1989. Petrology and emplacement dynamics of intrusive and extrusive rhyolites of Obsidian Dome, Inyo Craters Volcanic Chain, eastern California, *J. geophys. Res.,* **94**(B12), 17 937–17 956.

Waite, G.P., Chouet, B.A. & Dawson, P.B., 2008. Eruption dynamics at Mount St. Helens imaged from broadband seismic waveforms: interaction of the shallow magmatic and hydrothermal systems, *J. geophys. Res.,* **113**(B2), doi:10.1029/2007JB005259.

Yokoyama, I., 2005. Growth rates of lava domes with respect to viscosity of magmas, *Ann. Geophys.,* **48**(6), doi:10.4401/ag-8176.

Zorn, E.U. *et al.*, 2019. Load stress controls on directional lava dome growth at Volcán de Colima, Mexico, *Front. Earth Sci.,* **7,** 84, doi:10.3389/feart.2019.00084.